Desalination and Water Treatment
www.deswater.com

doi: 10.5004/dwt.2021.26764

215 (2021) 50–59
March

Evaluation of polyethersulfone microfiltration membranes embedded with MCM-41 and SBA-15 particles for turbidity removal

Mustafa H. Al-Furaiji[a,*], Khairi R. Kalash[a], Mohammed A. Kadhom[b], Qusay F. Alsalhy[c]

[a]*Environment and Water Directorate, Ministry of Science and Technology, Baghdad, Iraq, Mobile No. +964 7736792156; emails: m.h.o.alfuraiji@alumnus.utwente.nl (M.H. Al-Furaiji), khairirs@gmail.com (K.R. Kalash)*
[b]*Department of Environmental Science, College of Energy and Environmental Science, Alkarkh University of Science, Baghdad, Iraq, email: kadhom@kus.edu.iq*
[c]*Membrane Technology Research Unit, Chemical Engineering Department, University of Technology, Baghdad, Iraq, emails: qusay_alsalhy@yahoo.com/80006@uotechnology.edu.iq (Q.F. Alsalhy)*

Received 8 June 2020; Accepted 4 November 2020

ABSTRACT

In this work, mixed matrix polyethersulfone membranes were prepared and tested for turbidity removal. Mobil Composition of Matter No. 41 (MCM-41) and Santa Barbara Amorphous-15 (SBA-15) particles were filled inside the membranes to improve the performance in terms of turbidity rejection and water flux. Scanning electron microscopy, Mechanical strength, contact angle, Fourier-transform infrared spectroscopy, and performance test were conducted to investigate the prepared membranes. Results showed that embedding 1 wt.% of the silica additives led to an improvement in the water flux in the short-term operation. Here, the water flux increased from 200 L/m^2 h of the plain membrane to 252 and 240 L/m^2 h when the membranes loaded with MCM-41 and SBA-15, respectively, at an operating pressure of 0.5 bar. Interestingly, all membranes showed approximately a complete turbidity rejection (≥99.9%) at all examination conditions. However, backwash was employed to restore the original efficiency of the filled membranes; the regeneration was effective and the membranes gained almost their authentic status.

Keywords: Water filtration; Turbidity; Mixed matrix membranes; MCM-41; SBA-15

1. Introduction

In spite of the huge development in all life fields, the water crisis is an increasing danger that threatening beings due to the lack of traditional water resources [1]. Improving the conventional purification methods and finding new approaches and techniques to solve this issue are the main topics for many researchers and companies presently [2,3]. Also, other considerations such as the cost, simple operation, energy consumption, and environmental impact should be considered to come up with modified and integrated systems [4].

Microfiltration is a membrane process that is used in different applications, including water treatment, food and dairy industry, sterilization, and refinery processes, to sieve suspended solids in the size of 0.1–10 μm [5]. In water treatment, microfiltration is employed to purify rivers and lakes water from bacteria, contaminations, and turbidity, to produce potable water [6]. In many cases, microfiltration serves as a pre-treatment step for ultrafiltration, nanofiltration, and reverse osmosis processes, which maintains their membranes and produce high-quality water. Nevertheless, microfiltration is operated in a pressure range of 0.1–2 bar and has two types of design, dead-end and cross-flow filtration, where each is appropriate for certain types of applications [7].

* Corresponding author.

Although turbidity is resulted from different types of materials, such as colloids, particles, dissolved materials, and biomass, it is regulated to ≤1 NTU in most countries [8,9]. A high turbidity level means a higher prospect for people to gain gastrointestinal illnesses and other health problems [10]. In addition, high turbidity of surface water can affect the sustenance of organisms, fish, and aquatic plants [11].

Different methods were proposed for turbidity removal by many researchers. For instance, Daverey et al. [12] used banana peels and Indian bean seeds aqueous extractants as natural coagulants to remove turbidity, where the impact of contact time, amount of extractant, and pH were investigated. In both additives cases, 45 min, 0.6 mL/L, and pH of 11 were the optimum conditions to obtain 98.14% and 98.84% turbidity removal via banana peels and Indian bean seeds extractants, respectively. Asharuddin et al. [13] coupled cassava peel starch with alum and used them as coagulants to clear water from turbidity. Despite its low-cost and eco-friendly nature, the starch reduced both the used amounts of alum and settling time to half. Ultimately, the best turbidity removal efficiency was 91.47%.

Designing hybrid systems is another approach that was utilized by researchers. Here, Babaei et al. [14] employed three steps, multi-layer sand filtration, microfiltration, and ultra-filtration, a system to remove turbidity and other contaminations. The above-mentioned steps reduced the turbidity by 87.63%, 90.44%, and 98.91%, respectively, when they were separately operated. However, the three steps hybrid system efficiency reached up to 99.98%, where the outlet turbidity was 1.04 ± 0.8 NTU. Chen et al. [15] built a magnetic ion exchange resin and ultrafiltration hybrid system to eliminate the turbidity and organic micropollutant (carbamazepine). It was found that the hybrid system afforded better results than when the systems were individually operated.

Selecting the appropriate nanoparticles depends on the nanoparticles' properties and the membrane-process type; however, employing nanoparticles aims to enhance the performance of the membranes anyway. Silica NPs were widely used in water treatment as adsorbents and membranes' fillers.

In our work, we purified 500 NTU turbid water feed using a single step microfiltration system. Although the feed was not treated with any kind of pre-treatment, the permeate water was so clear with a system efficiency of ≥99.9% in all cases. Synthesizing membranes with the appropriate porosity was the key to purify water from the clay. To our best knowledge, adding Mobil Composition of Matter No. 41 (MCM-41) and Santa Barbara Amorphous-15 (SBA-15) silica nanoparticles into polyethersulfone (PES) membranes to remove turbidity was firstly investigated in this work, where they were found to be good improvers for the output flux without trading the rejection. Silica additives were selected due to their relatively low cost, easy preparation, and low health and environmental impact.

2. Materials and methods

2.1. Chemicals

The clay, that was used to prepare the feed solution, was collected from the beach of the Tigris River in Baghdad City, Iraq. PES (Mw = 150,000) was purchased from Macklin, Shanghai, China. N,N-dimethylformamide (DMF) was obtained from Fluka Chemie AG, Buchs, Switzerland. Cetyltrimethylammonium bromide (CTAB), Pluronic P123, and tetraethyl orthosilicate (TEOS) were obtained from Sigma-Aldrich, (Munich, Germany). Sulfuric acid was ordered from Biosolve, (Valkenswaard, The Netherlands). Sodium hydroxide (NaOH) and hydrochloric acid (HCl) were purchased from Thomas Baker, (India).

2.2. Preparation of MCM-41 particles

Non-calcinated MCM-41 microparticles were synthesized by adding 5.78 g of TEOS to a solution containing 0.34 g of NaOH and 1.01 g of CTAB in 30 g of deionized water. The solution was agitated for 60 min by a magnetic stirrer at room temperature and then crystallized at a temperature of 383 K using an autoclave for 96 h. The molar composition of the gel mixture was 1.0:0.1:0.3:60 of TEOS:CTAB:NaOH:H_2O, respectively. The solid product was recovered by filtration, washed by water several times to remove the organic template, and dried at 308 K for 24 h to prepare the non-calcinated MCM-41. Finally, the synthesized sample was calcinated at 823 K for 6 h in order to fully treat the product from the surfactant and template; at that point, a white powder was obtained [16].

2.3. Preparation of SBA-15 particles

HCl solution (180 g) of 2 molarity and 6.0 g of Pluronic P123 were dissolved in deionized water (45 g) at 308 K; then, 12.75 g of TEOS was added dropwise. The obtained mixture was agitated by a magnetic stirrer for 24 h at 308 K. Later, this mixture was matured by the oven at 373 K for 24 h. Finally, the product was filtrated, washed with distilled water to remove the residual surfactant, and dried at 373 K. As an ultimate point, the prepared sample was calcinated at the same conditions of MCM-41 calcination [17].

2.4. Preparation of the membranes

The membranes were prepared via the phase inversion phenomenon. Basically, PES polymer pellets were dissolved in DMF in a weight ratio of 15%, where the mixture was heated and stirred at 60°C for 6 h. The additives (i.e., MCM-41 and SBA-15 particles) were added to the casting solution with weight ratios of 0.5%, 1%, and 1.5% to synthesize the mixed matrix membranes (MMMs).

The product was a colorless solution that was cooled down at room temperature and left overnight for degassing. Later, an aliquot of the solution was spread on a glass plate and cast to 100 μm. The glass plate with the casted solution was immersed into a tub of water, where the solution turned to a white sheet immediately and detached from the glass in seconds. The prepared sheet was rinsed in the water at least three times to remove any trace of the solvent and stored in deionized water for at least 24 h before use.

2.5. Characterization methods

The morphology analysis of the prepared membranes was determined using a scanning electron microscopy

(SEM, VEGA3 – TESCAN, Czechoslovakia). Fourier-transform infrared (FTIR; IRPrestige-21, SHIMADZU, Japan) was used to impart details of the chemical bonds among the molecules. The mechanical properties were measured by conducting tensile tests using the Tinius Olsen device, England. Turbidity was measured using a turbidity meter (TurbidiDirect from Lovibond, Germany). The wettability of the membranes was studied by measuring the contact angle using a video system (Theta Lite TL-101, Thailand).

2.6. Membrane filtration performance

Microfiltration performance tests of the prepared membranes were conducted using a custom-built experimental setup. This system contains two tanks, one for feed and another for permeate collection. A diaphragm pump (from Pure-water®, China) was used to circulate the feed solution at a flow rate of 1 L/min and a pressure of 0.5 bar. The membrane was mounted in a custom-made cross-flow microfiltration cell that consists of two Perspex halves. The fluid in each halve flows in a rectangular channel with dimensions of 3 in length, 1 in width, and 1/8 in depth. Fig. 1 shows a diagram of the operation system.

Synthetic turbid water of 500 NTU turbidity was used as a feed solution in all experiments. This solution was prepared by adding 1.75 g of clay to 1 L deionized water with mixing for 60 min to ensure the homogeneous distribution. The water flux was calculated based on the permeate volume change per time throughout the experiment (5 h) using the following equation:

$$J_w = \frac{V_p}{A \times t} \tag{1}$$

where J_w is the water flux (L/m² h), V_p is the permeate volume (L), A is the membrane area (m²), and t is the experiment time (h).

The NTU rejection (R) was calculated by the following equation:

$$R = \left(1 - \frac{\text{NTU}_p}{\text{NTU}_f}\right) \times 100 \tag{2}$$

where NTU_p and NTU_f are the turbidities of permeate and the feed solution, respectively.

3. Results and discussion

3.1. Membrane characterization

3.1.1. FTIR test

The FTIR test was conducted to identify the chemical groups of the membranes and indicate the new groups due to additives influence. Fig. 2 elucidates the groups of the plain membrane (a), while (b) and (c) were after loading 1 wt.% of MCM-41 and SBA-15, respectively. From Fig. 2a, the peak at 3618 could be assigned to OH starching from the non-hydrogen bonds, while the peak at 3,549 cm^{-1} was attributed to OH stretching from the hydrogen bonds [18]. While the peak at 3,082 cm^{-1} and small peaks nearby could refer to CH aromatic stretching of the benzene ring [19]. The small peaks at the period 2,800–3,000 cm^{-1} could indicate CH_2 and CH_3 symmetric and asymmetric stretching from aromatic components [18]. However, they could indicate the OH stretching of aliphatic and aromatic species [20]. The peaks from 1,400–1,600 cm^{-1} could be assigned to the aromatic vibration [19]; more specifically, the peaks at 1,581 and 1,485 cm^{-1} point out to benzene ring stretch [20]. The peaks at 1,311 and 1,242 cm^{-1} may impute to COC stretching [19], where the 1,311 cm^{-1} peak represents CSO_2C asymmetric stretch [20]. The interval between 1,000–1,260 cm^{-1} contains peaks that could be attributed to CO asymmetric stretching [20], although the peaks at 1,103 and 1,157 cm^{-1} may refer to S=O stretching.

Fig. 2b shows the polymeric sheet embedded with MCM-41, where more peaks were generated. However, the peaks at 1,072 and 837 cm^{-1} could be related to Si–O–Si and Si–OH stretching vibrations, respectively [21]. While NH bending vibration could appear at 624 cm^{-1}. Fig. 2c had almost the same groups of the plain membrane except for the peak at 1,662 cm^{-1}, which could refer to the bending vibrations of the OH group of SBA-15.

3.1.2. SEM test

The morphology and cross-sectional views of the membranes were captured by the SEM device. Surface and cross-sectional views of the plain membrane were illustrated in Figs. 3a and b, respectively. While the 1 wt.% filled membranes were shown in (c) and (d) when MCM-41 was filled, and (e) and (f) in the SBA-15 case. From Fig. 3a, it can be noticed that the pores on the surface had a size of ≥700 nm.

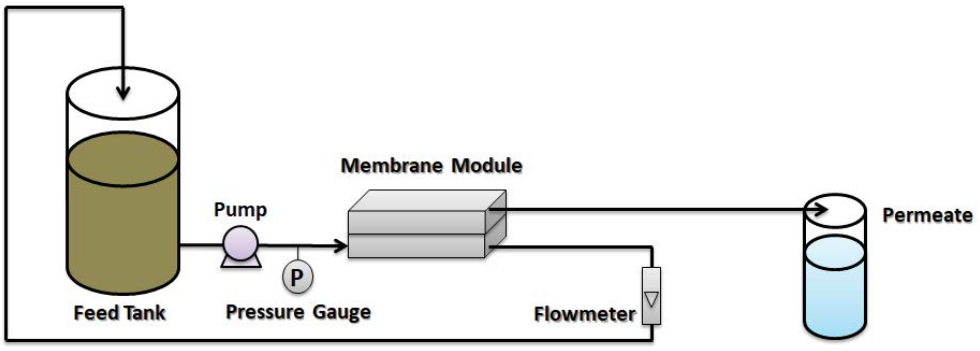

Fig. 1. Schematic diagram of the microfiltration bench-scale test unit.

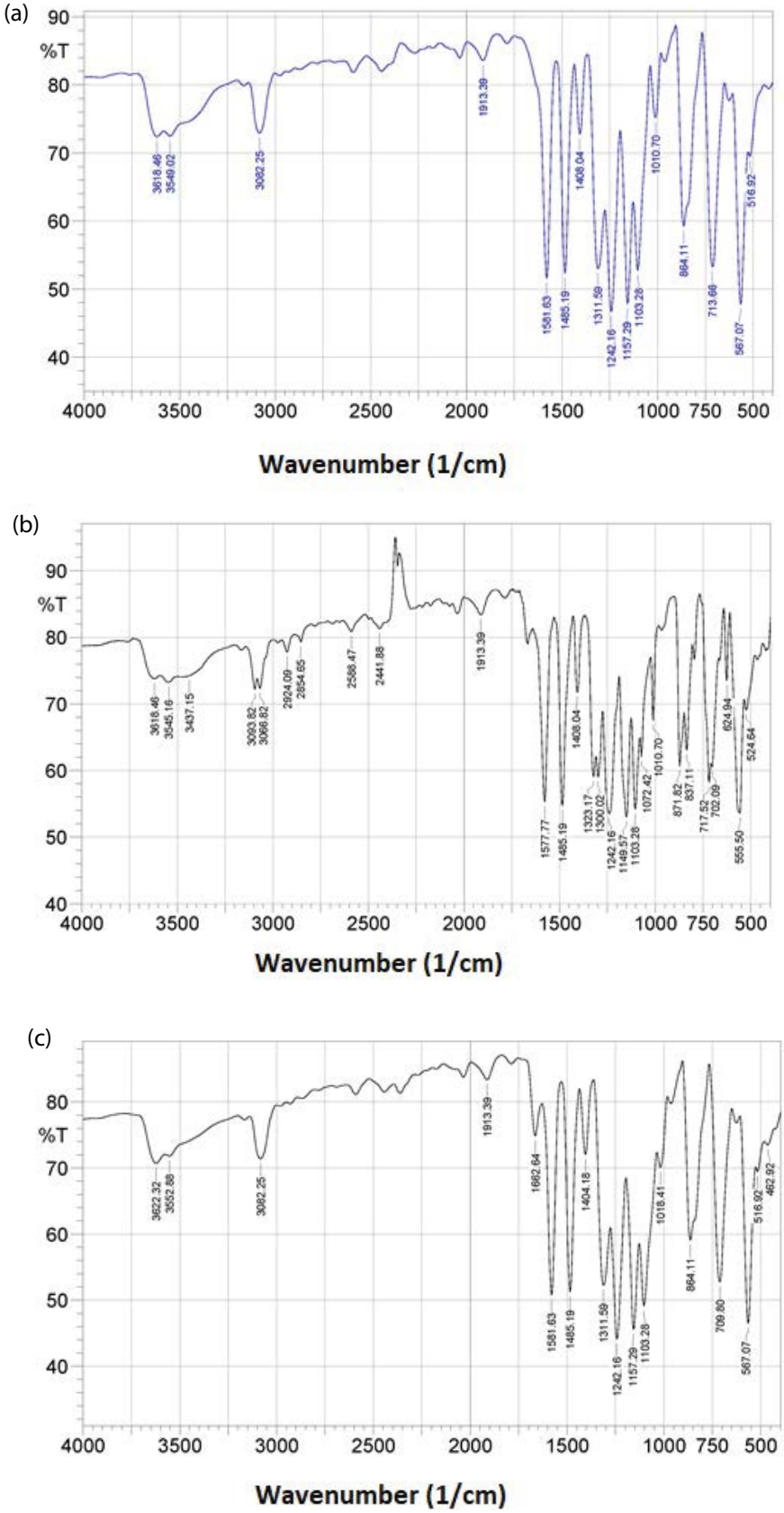

Fig. 2. Fourier-transform infrared spectroscopy test for (a) plain membrane, (b) 1 wt.% MCM-41 filled membrane, and (c) 1 wt.% SBA-15 filled membrane.

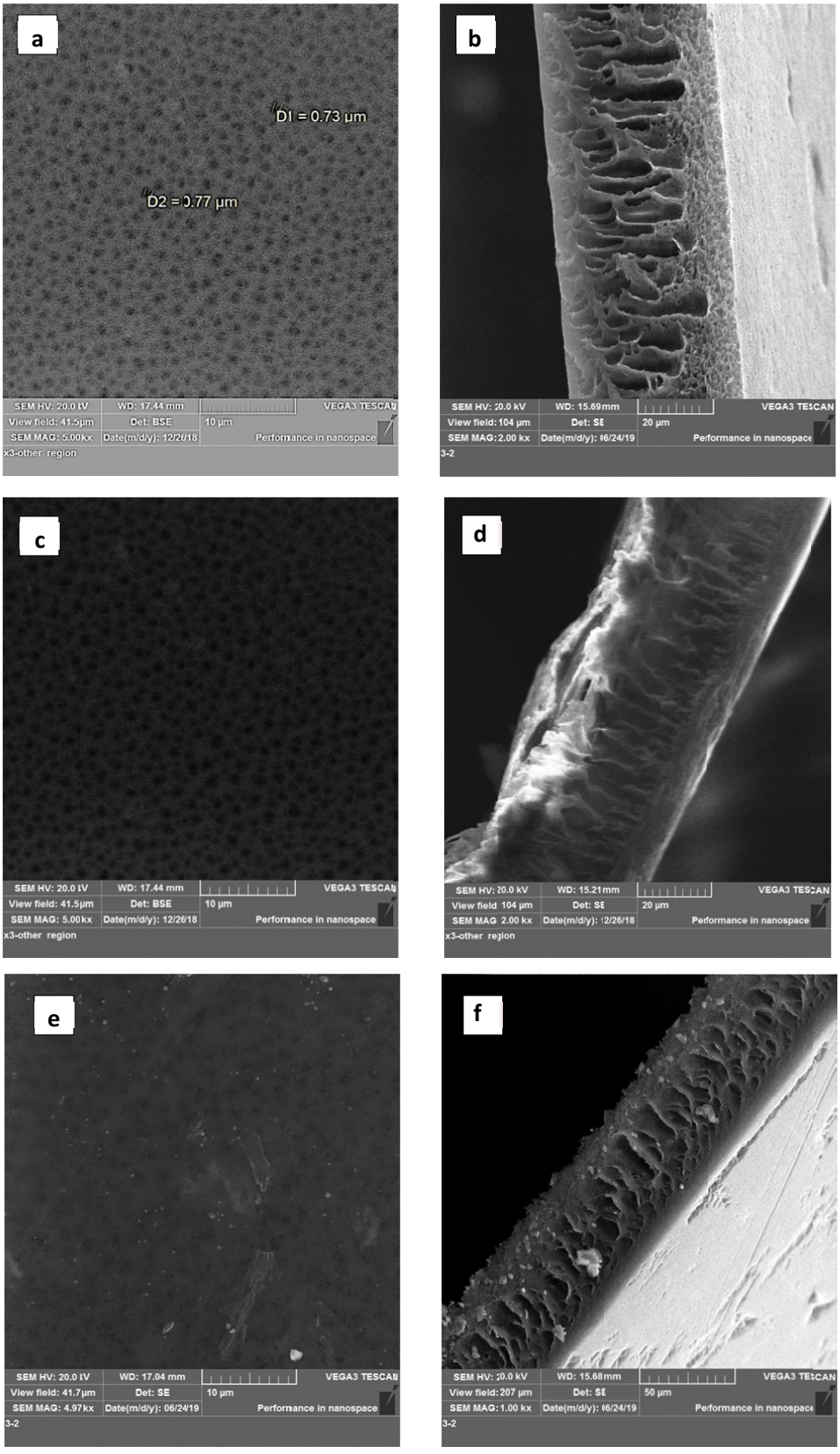

Fig. 3. SEM images of (a) PES plain top view, (b) PES plain cross-sectional view, (c) 1 wt.% MCM-41 PES membrane top view, (d) 1 wt.% MCM-41 PES membrane cross-sectional view, (e) 1 wt.% SBA-15 PES membrane top view, and (f) 1 wt.% SBA-15 PES membrane cross-sectional view.

The size and distribution of the pores seem homogenous, which gives high stability for the membranes under operation; this was confirmed by the performance test as shown in section 3–2. However, when the sheets were made of polysulfone (PSU) as reported in our previous work, the sheets showed a smaller pore size, around 100 nm [22]. This could be attributed to the polymer hydrophilicity, where the contact angles of the polysulfone and polyethersulfone are 84° and 79°, respectively [23]. As the PES is less hydrophobic, it could form wider pores due to its higher affinity to water. As the casting solution is immersed into the water, the solvent disperses and leaves the polymer to form a sheet depending on the hydrophobic nature of the polymer. As the PES is less hydrophobic than the PSU, the surface could less shrink, thus the pores on the surface were bigger.

The membranes' internal structure is shown in the cross-sectional images. Fig. 3b clarifies the plain membrane cavitation. From the image, the width of the cavities can reach up to 10 μm. Figs. 3c and d show the membrane after filling 1 wt.% of MCM-41, while (e) and (f) were for 1 wt.% SBA-15 membrane. The particles fitted inside the membranes and improved their physicochemical properties, as will be shown in other characterizations sections.

3.1.3. Contact angle test

The contact angle is used to measure the surface hydrophilicity, whereas a low contact angle refers to a high hydrophilic surface and vise versa. Fig. 4 shows the contact angle test, in which (a) refers to the plain membrane, (b) for the 1 wt.% MCM-41 membrane, and (c) for the 1 wt.% SBA-15 membrane. The plain membrane right and left contact angles were detected as 63.34° and 67.21°, respectively; so the average is 65.28°. Embedding 1 wt.% of silica nanoparticles inside the MMM led to an increase in the hydrophilicity, where the contact angles of MCM-41 and SBA-15 1 wt.% membranes were 59.53° (average of 60.61° and 58.44°) and 43.15° (average of 43.31° and 42.99°), respectively. This reduction in contact angle values is basically attributed to the hydrophilic nature of the silica, though it varied as two different types of silica were used. It was reported that the contact angles of MCM-41 and SBA-15 with pure water are 20.5° [24] and 18.9° [25], respectively. It is worth to mention that MCM-41's density is around double of SBA-15 [16,17]. Here, it can be presumed that although the contact angle values of the two silicas are very close to each other, respecting higher hydrophilicity for SBA-15, the SBA-15 altered the membrane's surface hydrophilicity to a higher degree than MCM-41. This could be attributed to SBA-15's lighter density, which may give a better distribution for the particles into the MMMs. Fig. 4 shows the contact angle test.

3.1.4. Mechanical properties

One of the main obstacles in polymeric membranes operation is the low mechanical endurance. The tensile strength can be defined as the ability of the material to hold an applied force without deformation. While the mechanical strain is the deformation measurement in terms of dimensions and particles' relative displacement of a solid object.

Embedding nanoparticles [26] and grafting and engineering polymers [27,28] inside the MMMs improved the membranes' mechanical properties. In our study, MCM-41 and SBA-15 silica nanoparticles were filled into the PES microfiltration membrane, and a tensile strength vs strain test was conducted. Fig. 5 shows the effect of embedding 1 wt.% of the additives on the strength and strain. Filling MCM-41 and SBA-15 increased the strength by 2.45 and 3 folds, respectively. The strain was also increased by 1.93-fold when MCM-41 was filled and 4.75 folds in SBA-15 case. This remarkable increase in mechanical properties refers to the improvement obtained by filling the silica additives. However, by considering the applied force and extension relationship of the membranes, it can be noted that the force increased in the order of SBA-15 > MCM-41 > plain. As a result, the extension increased by 1.94 and 4.77 folds for the MCM-41 and SBA-15 filled membranes, respectively, comparing to the plain membrane.

This improvement in the mechanical properties could be attributed to the high surface area and surface energy of the additives, in addition to many chemical groups on the silica surface that bond with the polymeric matrix. Specifically, the hydroxyl groups form hydrogen bonds with the matrix and enhance the membrane's rigidity [29]. It can be noted that SBA-15 had a higher impact than MCM-41; this is attributed to SBA-15's lower density that could give a higher distribution and less aggregation. However, both types of silica particles created a harmonious interface with the sheet and had a strong adhesion. Also, the extension was boosted by filling the additives; this could be assigned to pores formation, which made the sheet more plasticized [30]. The increase in the extension pursues the same order of stress, where the SBA-15 membrane had the longest extension, followed by the MCM-41 membrane, and lastly the plain membrane. Again, the SBA-15 could have a better distribution into the sheet matrix.

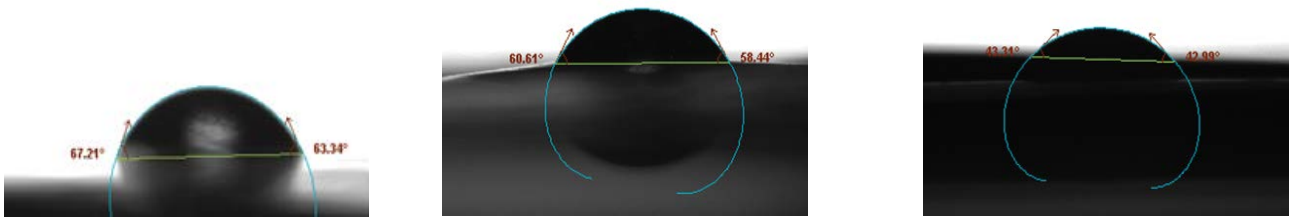

(a) (b) (c)

Fig. 4. Contact angle values for (a) plain membrane, (b) MCM-41, and (c) SBA-15.

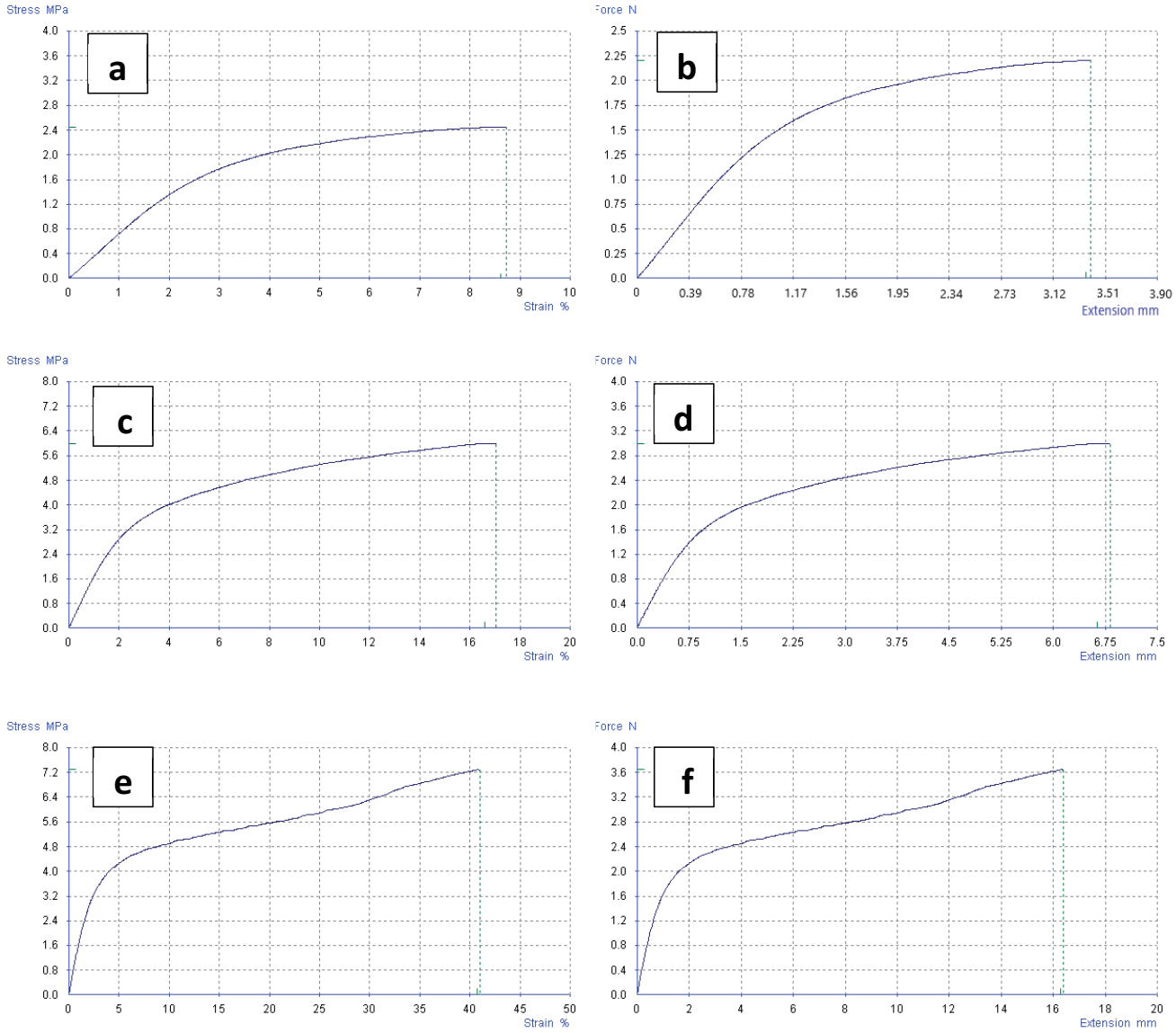

Fig. 5. Stress-strain and force-extension relationships of the plain membrane (a) and (b); 1 wt.% MCM-41 filled membrane, (c) and (d); and 1 wt.% SBA-15 filled membrane, (e) and (f), respectively.

3.2. *Membrane performance in microfiltration*

The MMM's performance was examined for short and long terms to identify their behavior before and after filling the silica additives. Fig. 6 shows the short-term operation (5 h) water flux of the plain and filled membranes with (a) MCM-41 and (b) SBA-15. Almost no change in the rejection was monitored (always > 99.9%), so the rejection comparison wasn't included. In Fig. 6a, MCM-41 particles were added in two loading ratios, 0.5 and 1 wt.%, where the performance of 1 wt.% MCM-41 MMM was the best, followed by 0.5 wt.% MCM-41 MMM, then the plain membrane. As the process run, the filled membranes flux decreases by time; however, the pristine membrane flux decreased at a slower rate. From Fig. 6b, similar behavior can be observed when SBA-15 particles were filled. Interestingly, MCM-41 MMMs showed better performance in terms of water flux than SBA-15 MMMs in both filling ratios, 0.5 and 1 wt.%. Also, the 0.5 wt.% MCM-41 MMM intersected the plain membrane flux line after 4 h of operation, further operation led to a diminution in flux. The same trend was obtained by 0.5 wt.% SBA-15 MMM, but the flux line intersection took place after around 3 h. Although the SBA-15 MMM showed higher hydrophilicity in the contact angle test, the MCM-41 MMM showed higher flux in the performance test. This could be attributed to the higher surface area of MCM-41 particles, which provides more space for water to pass through [31]. Another reason could be the shape of the internal pores, where the MCM-41 particle has a hexagonal shape but the SBA-15 has a circular. As MCM-41 hexagonal pores owe six straight lines and six corners, siloxane could form from the silanol group due to corners bending, which makes the channels more hydrophilic; Fig. 7 shows

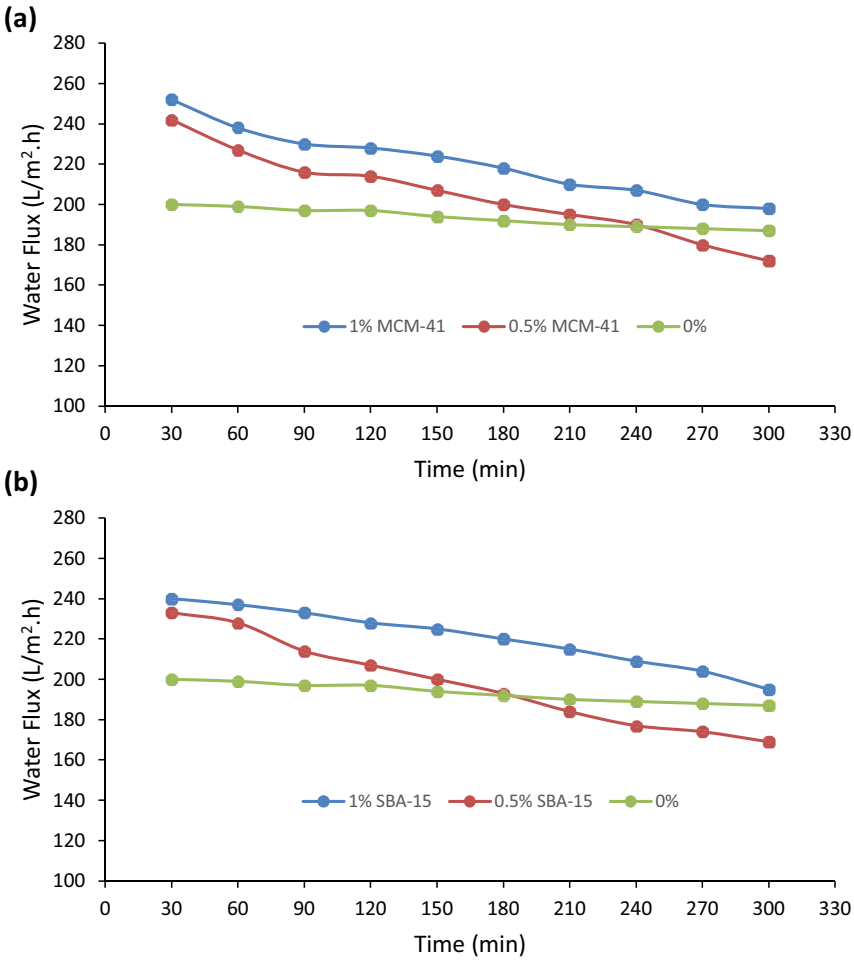

Fig. 6. Water flux relationship with time in a short-term operation mode for (a) MCM-41 filled membranes and (b) SBA-15 filled membranes.

the shape of the particles' pores [32]. The drop in flux after filling additives could be imputed to particles' pores blocking, which occurs by the turbid materials. Nevertheless, the reduction in flux was sharper for the 0.5 wt.% embedded membranes, and it was slightly improved by increasing the ratio of the particle. It is worth noting that filling 1.5 wt.% of the additives was tested, but sedimentation occurred while preparing the casting solution; thereby, it was excluded. Here, it can conclude that 1 wt.% addition gave the best performance; so, the long-term operation was examined for this ratio.

Fig. 8 shows the MMMs performance in long-term mode, where the 1 wt.% filled membranes were run for 1,300 min (around 22 h). Fig. 8a illustrates the plain membrane performance, while 8b and 8c are for MCM-41 and SBA-15 filled membranes, respectively. In the case of the additives-loaded membrane, backwashing was applied for 10 min after each 300 min operation period. Backwash was used due to the sharp drop in water flux comparing with the unmodified membrane. Despite the decrease in flux, which required utilizing backwash, the regenerated membranes regained their original status with a marginal reduction. However, MCM-41 MMM showed higher regeneration stability than the SBA-15 membrane. MCM-41 has a smaller pore size and wall thickness than SBA-15 [32], which could make turbidity cleaning from the membranes easier when backwashing is applied.

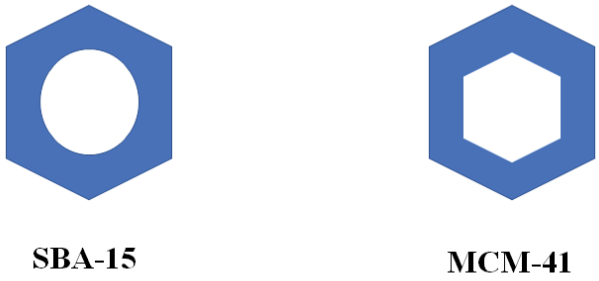

Fig. 7. The shape of internal pores of SBA-15 and MCM-41 silica particles.

4. Conclusions

In this work, turbidity removal was studied in a one-step filtration system. Filling MCM-41 and SBA-15 particles

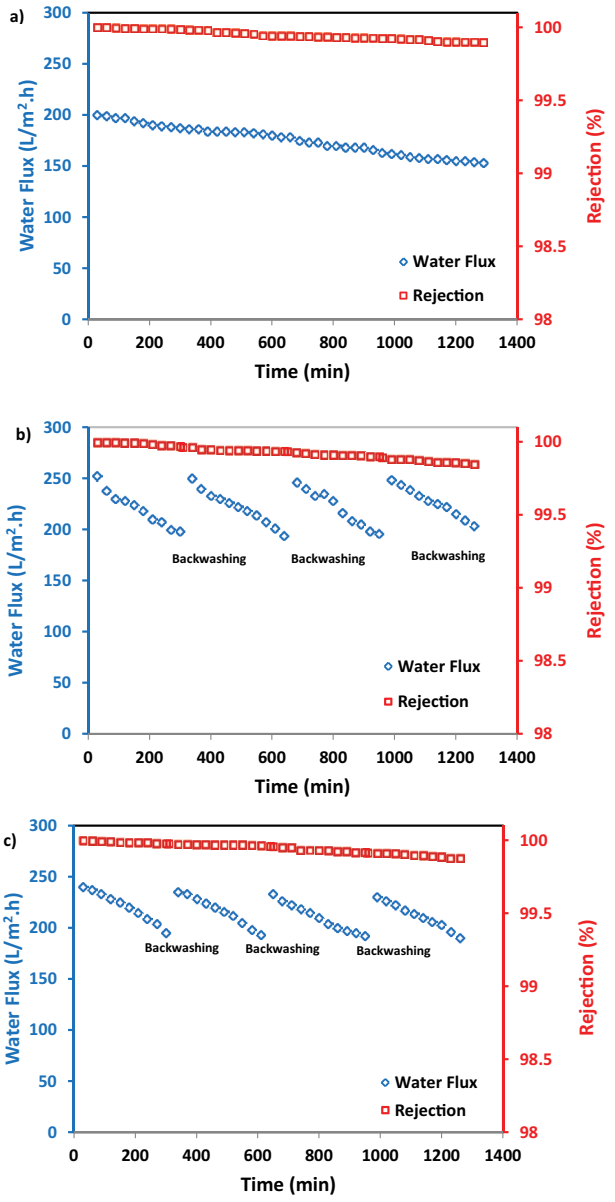

Fig. 8. Water flux and turbidity rejection relationship with operation time in a long-term operation mode for (a) plain membrane, (b) 1 wt.% MCM-41 filled membranes, and (c) 1 wt.% SBA-15 filled membranes.

into the MMMs was approached in situ during membranes preparation via the phase inversion technique. Silica particles improved the performance, where the flux enhanced by 20.6% and 16.7% by embedding 1 wt.% MCM-41 and SBA-15, respectively. However, the unmodified membranes were more stable in long-term operation than the modified membranes; thereby, backwash was applied when the filled membranes were tested. Turbidity rejection was not disturbed in all cases and maintained always ≥99.9%. Testing other types of particles and modifying the classic particles and membranes could be other topics to study. Also, using these types of membrane in heavy metal and oil removal could be an interesting area to investigate in.

Acknowledgment

The authors would like to thank the Ministry of Science and Technology in Iraq for partially supporting this project.

References

[1] K.R. Kalash, M.A. Kadhom, M.H. Al-Furaiji, Short-cut nitrification of iraqi municipal wastewater for nitrogen removal in a single reactor, IOP Conf. Ser.: Mater. Sci. Eng., 518 (2019) 022024, doi: 10.1088/1757–899X/518/2/022024.
[2] B.I.H. Waisi, U.F.A. Karim, D.C.M. Augustijn, M.H.O. Al-Furaiji, S.J.M.H. Hulscher, A study on the quantities and potential use of produced water in southern Iraq, Water Sci. Technol. Water Supply, 15 (2015) 370–376.
[3] M.H.O. Al-Furaiji, J.T. Arena, M. Chowdhury, N. Benes, A. Nijmeijer, J.R. McCutcheon, Use of forward osmosis in treatment of hyper-saline water, Desal. Water Treat., 133 (2018) 1–9.
[4] M. Elimelech, W.A. Phillip, The future of seawater desalination: energy, technology, and the environment, Science, 333 (2011) 712–717.
[5] R.W. Baker, Membrane Technology and Applications, John Wiley & Sons, Ltd., Chichester, UK, 2004.
[6] R.B. Klijn, W.G.J. van der Meer, H. Vriezen, F.H.J. van Ekkendonk, Surface water treatment with Zenon microfiltration membranes: minimisation of energy and chemical use, Desalination, 131 (2000) 337–343.
[7] L. Giorno, E. Piacentini, F. Bazzarelli, The Principle of Microfiltration, E. Drioli, L. Giorno, Eds., Encyclopedia of Membranes, Springer, Berlin, Heidelberg, 2015, pp. 1–4.
[8] T. Léziart, P.-M. Dutheil de la Rochere, R. Cheswick, P. Jarvis, A. Nocker, Effect of turbidity on water disinfection by chlorination with the emphasis on humic acids and chalk, Environ. Technol., 40 (2019) 1734–1743.
[9] V. Gauthier, B. Barbeau, G. Tremblay, R. Millette, A.-M. Bernier, Impact of raw water turbidity fluctuations on drinking water quality in a distribution system, J. Environ. Eng. Sci., 2 (2003) 281–291.
[10] A.G. Mann, C.C. Tam, C.D. Higgins, L.C. Rodrigues, The association between drinking water turbidity and gastrointestinal illness: a systematic review, BMC Public Health, 7 (2007) 256.
[11] M.E. Kjelland, C.M. Woodley, T.M. Swannack, D.L. Smith, A review of the potential effects of suspended sediment on fishes: potential dredging-related physiological, behavioral, and transgenerational implications, Environ. Syst. Decis., 35 (2015) 334–350.
[12] A. Daverey, N. Tiwari, K. Dutta, Utilization of extracts of *Musa paradisica* (banana) peels and *Dolichos lablab* (Indian bean) seeds as low-cost natural coagulants for turbidity removal from water, Environ. Sci. Pollut. Res., 26 (2019) 34177–34183.
[13] S. Mohd Asharuddin, N. Othman, N.S. Mohd Zin, H.A. Tajarudin, M.F. Md. Din, V. Kumar, Performance assessment of cassava peel starch and alum as dual coagulant for turbidity removal in dam water, Int. J. Integr. Eng., 10 (2018), doi: 10.30880/ijie.2018.10.04.029.
[14] F. Babaei, M.H. Ehrampoush, H. Eslami, M.T. Ghaneian, H. Fallahzadeh, P. Talebi, R.F. Fard, A.A. Ebrahimi, Removal of linear alkylbenzene sulfonate and turbidity from greywater by a hybrid multi-layer slow sand filter microfiltration ultrafiltration system, J. Cleaner Prod., 211 (2019) 922–931.
[15] Y.Y. Chen, W.Y. Xu, H.J. Zhu, D. Wei, F. He, D.S. Wang, B. Du, Q. Wei, Effect of turbidity on micropollutant removal and membrane fouling by MIEX/ultrafiltration hybrid process, Chemosphere, 216 (2019) 488–498.
[16] T.M. Albayati, K.R. Kalash, Polycyclic aromatic hydrocarbons adsorption from wastewater using different types of prepared mesoporous materials MCM-41 in batch and fixed bed column, Process Saf. Environ. Prot., 133 (2020) 124–136.
[17] T.M. Albayati, I.K. Salih, H.F. Alazzawi, Synthesis and characterization of a modified surface of SBA-15 mesoporous

silica for a chloramphenicol drug delivery system, Heliyon, 5 (2019) e02539.
[18] S. Belfer, R. Fainchtain, Y. Purinson, O. Kedem, Surface characterization by FTIR-ATR spectroscopy of polyethersulfone membranes-unmodified, modified and protein fouled, J. Membr. Sci., 172 (2000) 113–124.
[19] P. Qu, H.W. Tang, Y. Gao, L.P. Zhang, S.Q. Wang, Polyethersulfone composite membrane blended With cellulose fibrils, BioResources, 5 (2010) 2323–2336.
[20] A. Mushtaq, H. Bin Mukhtar, A. Mohd Shariff, FTIR study of enhanced polymeric blend membrane with amines, Res. J. Appl. Sci. Eng. Technol., 7 (2014) 1811–1820.
[21] M. Kadhom, J. Yin, B. Deng, A thin film nanocomposite membrane with MCM-41 silica nanoparticles for brackish water purification, Membranes (Basel), 6 (2016) 50, doi: 10.3390/membranes6040050.
[22] M. Kadhom, B. Deng, Synthesis of high-performance thin film composite (TFC) membranes by controlling the preparation conditions: technical notes, J. Water Process Eng., 30 (2019) 100542, https://doi.org/10.1016/j.jwpe.2017.12.011.
[23] E. Bormashenko, R. Pogreb, G. Whyman, Y. Bormashenko, R. Jager, T. Stein, A. Schechter, D. Aurbach, The reversible giant change in the contact angle on the polysulfone and polyethersulfone films exposed to UV irradiation, Langmuir, 24 (2008) 5977–5980.
[24] X. Diao, Y. Hu, Y. He, F. Quan, C. Wei, Preparation of 3,3,3-trifluoropropyl functionalized hydrophobic mesoporous silica and its outstanding adsorption properties for dibutyl phthalate, RSC Adv., 7 (2017) 8338–8346.
[25] Y.F. Pu, K. Xuan, F. Wang, A.X. Li, N. Zhao, F.K. Xiao, Synthesis of dimethyl carbonate from CO_2 and methanol over a hydrophobic Ce/SBA-15 catalyst, RSC Adv., 8 (2018) 27216–27226.
[26] J. Lv, S.L. Hu, H.S. Liu, D.M. Zeng, C. Wei, H. Lv, Mechanical and electrical properties of mesoporous MCM-41/unsaturated polyester *in situ* composites, Mater. Res. Innovations, 19 (2015) S1–199-S1–202.
[27] M. Al-Furaiji, J.T. Arena, J. Ren, N. Benes, A. Nijmeijer, J.R. McCutcheon, Triple-layer nanofiber membranes for treating high salinity brines using direct contact membrane distillation, Membranes (Basel), 9 (2019) 60, https://doi.org/10.3390/membranes9050060.
[28] L.W. Huang, J.T. Arena, S.S. Manickam, X.Q. Jiang, B.G. Willis, J.R. McCutcheon, Improved mechanical properties and hydrophilicity of electrospun nanofiber membranes for filtration applications by dopamine modification, J. Membr. Sci., 460 (2014) 241–249.
[29] S.S. Swain, L. Unnikrishnan, S. Mohanty, S.K. Nayak, Gas permeation and selectivity characteristics of PSf based nanocomposite membranes, Polymer (Guildf), 180 (2019) 121692, https://doi.org/10.1016/j.polymer.2019.121692.
[30] X. Yang, H. Liu, Y.J. Zhao, L.F. Liu, Preparation and characterization of polysulfone membrane incorporating cellulose nanocrystals extracted from corn husks, Fibers Polym., 17 (2016) 1820–1828.
[31] K. Kalash, M. Kadhom, M. Al-Furaiji, Thin film nanocomposite membranes filled with MCM-41 and SBA-15 nanoparticles for brackish water desalination via reverse osmosis, Environ. Technol. Innovation, 20 (2020) 101101, https://doi.org/10.1016/j.eti.2020.101101.
[32] H.-P. Lin, C.-Y. Tang, C.-Y. Lin, Detailed structural characterizations of SBA-15 and MCM-41 mesoporous silicas on a high-resolution transmission electron microscope, J. Chin. Chem. Soc., 49 (2002) 981–988.